Journal Pre-proof

Model sensitivity of Tibetan Plateau surface potential vorticity and the Asian summer monsoon system to Asian orographic perturbation in FGOALS-f2

Bian He , Yimin Liu , Qing Bao , Guoxiong Wu , Chen Sheng , Xiaoqi Zhang , Xinyu He

PII: S2667-3258(23)00312-6
DOI: https://doi.org/10.1016/j.fmre.2023.08.013
Reference: FMRE 648

To appear in: *Fundamental Research*

Received date: 9 February 2023
Revised date: 31 July 2023
Accepted date: 21 August 2023

Please cite this article as: Bian He , Yimin Liu , Qing Bao , Guoxiong Wu , Chen Sheng , Xiaoqi Zhang , Xinyu He , Model sensitivity of Tibetan Plateau surface potential vorticity and the Asian summer monsoon system to Asian orographic perturbation in FGOALS-f2, *Fundamental Research* (2023), doi: https://doi.org/10.1016/j.fmre.2023.08.013

Model sensitivity of Tibetan Plateau surface potential vorticity and the Asian summer monsoon system to Asian orographic perturbation in FGOALS-f2

Bian He[1,2], Yimin Liu[1,2], Qing Bao[1,2], Guoxiong Wu[1,2], Chen Sheng[1,2], Xiaoqi Zhang[3,1], Xinyu He[1,2]

[1]State Key Laboratory of Numerical Modeling for Atmospheric Sciences and Geophysical Fluid Dynamics (LASG), Institute of Atmospheric Physics (IAP), Chinese Academy of Sciences, Beijing 100029, China.

[2]University of Chinese Academy of Sciences, Beijing 100029, China.

[3]Nanjing University of Information Science and Technology, Nanjing 210044, China.

Corresponding author: heb@lasg.iap.ac.cn (B. He)

Submitted to *Fundamental Research*

Abstract

The thermodynamic forcing of the Tibetan Plateau (TP) is important for the regulation of the Asian summer monsoon (ASM). However, the monsoon responses to orographic perturbation simulations show controversial results in previously published literature. One reason for this is that the monsoon responses to orographic forcing differ among climate models. Another reason is that the quantitative changes in the TP thermodynamic forcing remain unknown when the orography is modified. Therefore, the relationship between the TP forcing and the ASM may be different among climate models. In this paper, the surface potential vorticity (SPV) is used to quantify the surface thermodynamic forcing on the TP in the FGOALS-f2 climate model for both the standard Atmospheric Model Intercomparison Project (AMIP) and Coupled Model Intercomparison Project (CMIP) experiments with a modified orography, and various aspects of the ASM responses are also examined. Finally, their relationships with TP-SPV changes are quantitively estimated. The results indicate that

the intensity of TP-SPV is reduced by nearly 100% in the AMIP runs, while it is reduced by 68% in the CMIP runs when the Asian mountains are removed. Overall, the responses of the monsoon system are more sensitive when air-sea interactions are considered. When the mountains are removed, the precipitation over the southern slope of the TP decreases by 73% and increases by nearly 30% over the tropical Indian Ocean in the CMIP runs. Moreover, the precipitation responses exhibit the largest difference between the AMIP and CMIP runs over the East Asian and Western Pacific regions. The precipitation over the Western Pacific remains almost unchanged when the orography is removed in the AMIP runs but is reduced by 20% in the CMIP runs. We propose that the calculation of SPV over the TP is helpful for understanding the TP orographic forcing and monsoon dynamics in the future.

Keywords: Tibetan Plateau, Asian summer monsoon, model sensitivity, potential vorticity, thermal forcing

1. Introduction

The climate model is a powerful tool to understand climate change during the past and present and to predict the future. The development of climate models dates back to the mid-20th century. Early studies [1,2] attempted to solve the barotropic vorticity equation by numerical integration and produced weather forecasts for the 500 hPa geopotential height. They also tried to reduce the forecast error that originates from the algorithm of the finite-difference equations by constructing the “equivalent-barotropic” atmosphere and the geostrophic approximation. The orography on Earth is recognized as an important external forcing and boundary condition for the numerical model. In the equivalent-barotropic model, the large-scale orography could perturb the atmosphere and trigger gravity waves, Rossby waves and other waves that could influence the weather and climate system [3-5]. A typical example is the largest topography in the world, the Tibetan Plateau (TP), which has a great influence on the background westerly wind and forms the downstream East Asian jet [5]. Moreover, the numerical simulations carried out by Hahn and Manabe [6], in which the TP orography was removed in an 11-level numerical model, found that the Asian summer monsoon (ASM) retreated southward to the Indian Ocean instead of moving northward and inland to Asia. The finding that, without the dominant blocking effect of the TP, the monsoon flow moves southward rather than northward surprised the scientific community. Later studies [7,8] proposed that the sensible heating of the TP is the major driving force in the transport of abundant water vapor from the ocean surface to the land, leading to monsoonal precipitation over the Asian continent, known as the sensible heat-driven air pump (SHAP). In these studies, they found that sensible heating on the sloping lateral surface, rather than plateau heating, appeared to be the major driving source in idealized aqua-planet experiments.

Along with the development of climate system models, a series of standardized experiments have been organized by the World Climate Research Programme (WCRP) to understand model biases and to improve our understanding of the climate system since the

1980s. There are two most popular model intercomparison projects that have been widely used. The first is the Atmospheric Model Intercomparison Project (AMIP) proposed by Gates [9]. In this kind of experiment, the atmospheric model is forced by the observed sea surface temperature (SST) and sea ice concentration. The second is the Coupled Model Intercomparison Project (CMIP), which was launched in the 1990s. The CMIP experiments were performed by using a fully coupled model including the atmosphere, dynamic ocean, land surface, and thermodynamic sea ice components [10,11]. Regarding the influence of the TP on the Asian summer monsoon determined by the climate model, sensitivity experiments related to TP thermodynamic perturbations have been carried out in both AMIP and CMIP simulations in recent decades. In general, the model results and conclusions are consistent across most aspects but not all of them. For example, removing the TP orography in AMIP or CMIP experiments has been carried out by many models after Hahn and Manabe [6], and their results and conclusions have been quite consistent, i.e., that the Asian summer monsoon will retreat to the Indian Ocean if the TP is removed. These results highlight that the existence of the TP is crucial for the maintenance of the ASM [12-31]. Furthermore, the uplift of the Himalayas and TP has been recognized as the dominant forcing for the gradually established ASM over the southern TP and East Asian land by testing different altitudes and horizonal scales of the TP orography in numerical models [32,13,14,16].

However, the relative role of the TP thermal and dynamic forcing on ASM formation has been debated over recent decades because the sensitivity simulation to the Asian orographic perturbation is quite different. Boos and Kuang [33,20] found that only the simulated ASM pattern with the presence of the Himalaya Mountains is similar to the pattern in the control run when the orography is not changed by using version 3 of the Community Atmosphere Model (CAM3). Wu et al. [23] and He et al. [25] further noted that the elevated heating on the south slope is still retained in these experiments. They further removed the slope heating of the Himalayas in a Spectral Atmospheric model of IAP LASG (SAMIL) and found that the Asian land monsoon precipitation and wind response, which are associated with the high surface entropy at the foot of the Himalayas, have all been substantively suppressed. Additionally, some numerical studies revealed that the TP thermal forcing could influence the ASM variability through air-sea interactions in simulations of the coupled general circulation model (CGCM) [34,26,27]. Moreover, other studies found that the monsoon responses greatly differ when the TP orography is modified in different approaches [35,36,24,29-31]. One reason for these differences is that the model responses to the same orographic forcing may be sensitive and different. Another reason is that the experimental designs for the TP orography and thermal property modifications also have large influences on the simulation results.

Although many orographic perturbation experiments have been carried out to understand the TP dynamics, none of these studies discussed how the TP thermodynamic forcing changes when the orography is modified in the model. For example, in simulations when TP orography is removed, the blocking effect of the mountains and the elevated heating effect disappear, but non-elevated heating still exists. The differences between the simulations with and without TP orography are the model responses to the TP thermodynamic forcing changes.

These changes may be different across a variety of models due to the diverse model sensitivity. To understand the TP thermodynamic forcing changes in the climate, He et al. [37] recently proposed a new method by using potential vorticity instead of sensible heat flux to quantitively understand the changes in TP surface thermodynamic forcing. They showed that the TP surface potential vorticity (TP-SPV), which includes the topographical effect, near-surface absolute vorticity, and land–air potential temperature differences, could well depict the seasonal variations in the TP thermal status and has a good relationship with ASM development. Therefore, in this study, we aim to diagnose the TP thermodynamic forcing changes, Asian summer monsoon system response and their relative relationships in the FGOALS-f2 climate model by calculating TP-SPV and many other indices related to ASM to understand the model sensitivity to perturbed orography in both AMIP and CMIP simulations. The results will be helpful for both model development and the advancement of TP dynamic studies. The rest of this paper is structured as follows: Section 2 introduces the methods, model and experimental design used in this study. Section 3 presents the model responses in the AMIP and CMIP experiments. Finally, the conclusions and discussion are provided in Section 4.

2. Methods, model and experimental design

2.1 Methods

For simplicity, the SPV used in this study is shown as follows in Eq. 1 ($PV^*_{\sigma_1}$). A more detailed derivation process can be found in He et al. [37].

$$PV^*_{\sigma_1} = -PV_{\sigma_1} = -\left[-\frac{g}{ps}\left(f+\zeta_{\sigma_1}\right)\frac{\theta_s-\theta_a}{1-\sigma_1}\right] \quad (1)$$

Here, σ_1 denotes the first σ level above the surface of the Earth, which is the bottom level of the atmospheric model; ζ_{σ_1} is the relative vorticity at the σ_1 level; θ_s is the potential temperature at the surface of the Earth; ps is surface pressure, and θ_a is the air potential temperature at the σ_1 level. In terrain-following coordinates, the SPV along the TP surface becomes a horizontally integrated SPV along the σ surface. Thus, the calculation of the total SPV over the TP surface on the σ surface can be used to determine the integrated intensity of the TP thermodynamic forcing. Based on Eq. 1, we defined an index for the estimation of the total TP surface thermodynamic forcing (TP-SPVI) on a σ surface:

$$I_{TP} = \iint PV^*_{\sigma_1}\,dxdy = \iint -\left[-\frac{g}{ps}\left(f+\zeta_{\sigma_1}\right)\frac{\theta_s-\theta_a}{1-\sigma_1}\right]dxdy \quad (2)$$

In this study, the TP region we focus on mainly covers the area ranging from 25°N–40°N and 70°E–110°E with an elevation above 3000 m, shown as the black contour in Fig. 1. Therefore, in the following section, Eq. 2 is used for the above domain to measure the TP thermodynamic forcing changes in the numerical experiments.

2.2 Model introduction

The climate model we used here is the Chinese Academy of Sciences (CAS) Flexible Global Ocean-Atmosphere–Land System model, finite-volume version 2 (CAS FGOALS-f2), which was developed at the State Key Laboratory of Numerical Modeling for Atmospheric

Sciences and Geophysical Fluid Dynamics (LASG), Institute of Atmospheric Physics (IAP). It is composed of five components: Version 2.2 of the Finite-volume Atmospheric Model (FAMIL) [38-40,26,27]; version 2 of the Parallel Ocean Program (POP2) [41]; version 4.0 of the Community Land Model (CLM4) [42]; version 4 of the Los Alamos sea ice model (CICE4) [43]; and version 7 of the coupled module from the National Center for Atmospheric Research (NCAR) (http://www.cesm.ucar.edu/models/cesm1.0/cpl7/), which is used to exchange the fluxes among these components.

The atmospheric component, FAMIL, uses the finite-volume dynamical core [44] on a cubed-sphere grid [45]. The resolution used in this study is approximately equal to a 1° horizontal resolution. In the vertical direction, the model uses hybrid coordinates over 32 layers, with the top of the model at 2.16 hPa. The main physical packages include a new moisture turbulence parameterization scheme for the boundary layer [46], with updated shallow convection [47]. The Geophysical Fluid Dynamics Laboratory (GFDL) version of the single-moment six-category cloud microphysics scheme is also applied [48,49]. A semiempirical scheme that mainly uses the large-scale average condensate mixing ratio as the primary predictor is used for cloud fraction diagnosis [50]. A resolving convective precipitation parameterization (©2017 FAMIL Development Team) is used, where in contrast to the conventional convective parameterization, convective and stratiform precipitation are explicitly calculated. The rapid radiative transfer model for GCMs (RRTMG) [51] is introduced into the model as the main radiation transfer. A gravity wave drag scheme is also used based on the methods of ref. [52].

2.3 Experimental design

To understand the model sensitivity to the large-scale Asian mountain perturbation, two routine types of experiments, AMIP and CMIP simulations, are used as control runs here. Simplified experimental settings and their differences are provided in Table 1. Since the model participated in the CMIP6 project [53], the AMIP r1i1p1f1 experiment of the FGOALS-f2 climate model in the Diagnostic, Evaluation and Characterization of Klima (DECK) is directly used here for the control run. In this type of experiment, the model is forced by the observed SST and sea ice, with an integration from 1970 to 2014, where the first 9 years are considered the spin-up time and the results from 1979 to 2014 are provided for analysis. Since the JJA mean values are analyzed in this study, there are 36 samples for the statistical calculation. Other information, such as the external forcing datasets, can be found in He et al. [26].

The second experiment is the AMIP-TIP (renamed A_NTP in Table 1 and used hereafter) experiment of the FGOALS-f2 model in the Global Monsoons Model Intercomparison Project (GMMIP) Tier-3 experiments [54]. The topography above 500 m is set to 500 m in the Tibetan and Iranian (TIP) region during integration in this experiment. Other configurations are exactly the same as those in the AMIP run, as documented above.

The third experiment is a fully coupled run named CMIP, as shown in Table 1. In this type of experiment, the SST and sea ice are simulated in the model. The model runs a 500-year integration as the spin-up run. Then, the model is restarted from the spin-up run for

an additional integration for 100 years, and the last 50 years are used here for analysis. Therefore, there are 50 samples available for the statistical calculation. Other forcing datasets are the same as the standard piControl simulations [55].

The fourth experiment (C_NTP in Table 1) is also a fully coupled run, but the TIP orography is removed in the model, which is the same as in A_NTP. Other experimental settings are the same as in the CMIP run as documented above.

Additionally, the differences between the AMIP and A_NTP are denoted by A_DIF, while the differences between the CMIP and C_NTP are denoted by C_DIF. If we define V_1 as the TP-SPV value in AMIP and V_2 as the TP-SPV value for A_DIF, then the quantitative calculation of the percentage changes in TP-SPV for the AMIP-type run, which is denoted by R_A here, can be expressed as follows:

$$R_A=V_2/V_1*100 \quad (3)$$

This value is shown in the middle column and the second row in Table 2. Similarly, the percentage changes in various precipitation and circulation indices are also calculated by the above formula and shown in other rows in the middle column of Table 2. In the CMIP type run, we define V_{1C} as the TP-SPV value in CMIP and V_{2C} as the TP-SPV value for C_DIF. Then, the quantitative calculation of the percentage changes of TP-SPV, which is denoted as R_C, can be expressed as

$$R_C=V_{2C}/V_{1C}*100 \quad (4)$$

The relative values for various indices are shown in the right column in Table 2.

To understand the relative changes of the monsoon precipitation to the TP-SPV percentage changes, the relative ratios of precipitation changes in AMIP and CMIP type runs, which are listed from row 3 to row 7 in Table 2, are calculated as follows:

$$R_{RA}=R_{VA}/R_A*100 \quad (5)$$

$$R_{RC}=R_{VC}/R_C*100 \quad (6)$$

where R_{RA} and R_{RC} denote the relative changes in precipitation to the changes in TP-SPV in the AMIP and CMIP types runs, respectively. R_{VA} and R_{VC} represent the percentage changes in precipitation as calculated by formulas (3) and (4), respectively. R_A and R_C are the TP-SPV percentage changes for the AMIP and CMIP types of runs, respectively.

3. Results

3.1 SPV responses

The June-July August (JJA) mean SPV simulated in the AMIP run is shown in Fig. 1a. It is clear that the SPV maxima appear mainly over the middle to western TP and adjacent mountain regions. The SPV over the flat regions of the Eura-Asian continent is relatively small and even negative in the northern high latitudes. For the simulated SPV in the fully coupled run (CMIP run, Fig. 1d), the climate mean SPV shows overall strong positive values over the entire TP (contoured by 3,000 m of the orographic altitude) and positive values over most of the Eura-Asian continent. Therefore, both simulations could capture the basic pattern of SPV during boreal summer compared to the reanalysis (Fig. 2 in He et al., [37]). However, we need to note that the SPV is strongly negative (lower than -8 PVU) at high latitudes in the AMIP run but weakly negative (close to -2 PVU) in the CMIP run, which could be attributed

to the effect of air-sea interactions. Another difference is also clear. The SPV shows an overall stronger pattern in the mid-west part of the TP in the AMIP and CMIP runs, while the east–west contrast is more prominent in the AMIP run. This result implies that the SPV over the eastern TP is more sensitive to the modulation of air-sea interactions.

When the TIP topography is removed in the experiments, the SPV also changes accordingly. As shown in Fig. 1b, the SPV shows very small values over the existing TP (contoured by dashed line), and the distribution is also similar in the C_NTP run (Fig. 1e), except that the SPV is overall slightly stronger than that in the A_NTP run over the whole Eura-Asian continent. This result indicates that the thermodynamic forcing of the TIP region is substantively suppressed by removing the topography. The differences between the AMIP and A_NTP and between the CMIP and C_NTP are shown in Fig. 1c and 1f, respectively. It is clear that the SPV differences appear as striking positive values over the TP in both fields, which indicates that the topographical thermodynamic forcing over the Eura-Asian continent is mainly controlled by the TP.

To quantitatively understand the thermodynamic forcing changes and the associated data distributions that occur by removing the topography in the experiment, we show the boxplot for the regional (3,000 m contour line in Fig. 1a) sum of the SPV in Fig. 2. The results show that in the AMIP run, the sum of the SPV over the TP reaches 1,300 to 2,000 PVU with a mean of approximately 1,700 PVU. When the topography is removed, the SPV (regional sum where the elevation is above 3,000 m) is reduced to nearly 0 and even negative in the A_NTP run. The distributions of the SPV also decrease with a range from -2 to 2 PVU. This result suggests that the overall TP thermodynamic forcing is suppressed in the A_NTP run. The SPV shows a larger distribution from 1,500 to 2,500 PVU in A_DIF, with a mean value of approximately 2,000, which is 123% times that of the AMIP run. This result implies that the TP thermodynamical forcing is quite sensitive to the changes in orography in the AMIP simulation. For the fully coupled runs, the SPV in CMIP ranges from 1,800 to 2,300 PVU, with a mean value close to 2,000 PVU. It seems that the TP forcing is slightly stronger in the CMIP than in the AMIP. Surprisingly, when the topography of the TIP region is removed in the coupled run, the SPV is reduced to approximately 520 PVU at the TP location and is approximately 32% of the total SPV in the CMIP simulation. This means that almost one-third of the surface forcing is still retained when the topography is removed. This is quite different from a previous study that found that the changes in sensible heat fluxes are almost the same when the topography of the TIP is modified in both AGCM and CGCM runs [27]. The SPV changes in C_DIF range from approximately 1,200 to 1,900 PVU, with a mean value of 1,500 PVU, which accounts for 75.5% of the SPV in the CMIP run. The differences in SPV changes between the CMIP and AMIP experiments reveal that air-sea coupling could compensate for the local surface thermodynamics effects when the topography is removed in the model.

3.2 Monsoon precipitation and western Pacific High responses

Precipitation and 850 hPa winds are the two key elements for measuring the ASM. As shown in Fig. 3a and evaluated in He et al. [26], the basic patterns of precipitation and winds

that are simulated in the AMIP run show a reasonable pattern of the ASM, with three strong precipitation centers over the Arabian Sea, Bay of Bengal, and northwestern Pacific. However, the AMIP run overestimates the precipitation over ocean regions and underestimates the precipitation over East Asian land. This bias is reduced to some extent in the CMIP run (Fig. 3d), which implies that the air-sea interaction could help the model obtain a more realistic land–sea thermal contrast and produce a more reasonable ASM precipitation pattern. When the topography of the TIP region is removed, the southern precipitation branch of the SASM still exists and is also accompanied by strong westerlies over the northern Indian Ocean in both A_NTP and C_NTP. However, the precipitation over Asian land regions becomes weak, and specifically, the strong precipitation over the southern TP is completely gone, which could be attributed to the removal of the pumping effects of the TP.

The western Pacific High (WPH) is another important large-scale climate system that is greatly associated with changes in the ASM. The west–east shift of the WPH could lead to changes in water vapor transport over East Asian land and influence the tropical cyclone track in the western Pacific. Here, we use the contour of the 1485 geopotential height at 850 hPa to represent the boundary of the WPH in the model (the model systematically underestimates the WPH intensity at 500 hPa), as shown by the red contour in Fig. 3. The western boundary of the WPH is located over 150 °E in the AMIP run (Fig. 3a), which is also quite close to the position simulated in the CMIP run (Fig. 3b). When the TIP is removed, the western boundary of the WPH moves slightly westward to approximately 140 °E in A_NTP (Fig. 3b), while it moves to almost 130 °E in C_NTP and is accompanied by a clear reduction in precipitation and a weakening of winds (Fig. 3e). The above results also indicate that the simulation of the WPH is quite sensitive in the fully coupled run and could influence the simulation of the water vapor transport from the western Pacific.

The precipitation and 850 hPa wind responses to the thermodynamic forcing of TIP can be directly derived by the differences between the AMIP and A_NTP (A_DIF, Fig. 3c) and the CMIP and C_NTP (C_DIF, Fig. 3f). The precipitation anomaly in A_DIF is mainly strongly positive over the South Tibetan Plateau, South Asian flat land, and Bay of Bengal. It also appears positive over East Asian land, the South China Sea, and the western Pacific. Meanwhile, the precipitation mainly decreases over tropical Indian Ocean regions, accompanied by the *in situ* east wind anomaly. Dynamically consistent with the increases in precipitation, the 850 hPa wind mainly shows a cyclonic anomaly around the TP, featuring enhanced westerlies over the northern Indian Ocean and South Asian land and enhanced meridional wind over East Asian land. Corresponding to the thermodynamic forcing in the TIP region, the response of geopotential height at 850 hPa (contour in Fig. 3c) shows a strong negative anomaly around the TP and extends to the Indian Ocean and western Pacific regions. All the above model responses suggest that a large-scale thermal low pressure is the basic climate system response induced by the forcing in the TIP region. For the model response in the fully coupled run (Fig. 3f), the C_DIF shows a large-scale pattern similar to that of the A_DIF for both circulation and precipitation. However, some striking differences also appear. For example, there is a greater precipitation increase over East Asian land and the western Pacific in C_DIF than in A_DIF, which implies that the role of air-sea interactions could

amplify the forcing effect in the TIP region on Asian climate change.

Despite the differences between the A_DIF and C_DIF, the large-scale response pattern over South Asia is basically reproduced with different climate models in many previous studies [56,6,14,15,20,23,24,26,29-31]. However, magnitude and regional differences in the ASM responses still existed, which could lead to different understandings of the TP climate effect. The discrepancy could be attributed to the model sensitivity to orographic forcing, which is related to the dynamic and physical configuration and the experimental design of the model. Thus, a quantitative calculation of the monsoon response in the model experiment is the first step to understanding the causes of the difference within the different experiments. Because precipitation is a key metric to measure the intensity of the ASM changes and its spatial pattern is quite inhomogeneous, we calculate five regional means (blue boxes in Fig. 3c and f) of precipitation changes to indicate the monsoon precipitation responses in different ASM areas. These regions include the south Tibetan Plateau (STP, 25-32°N, 75-105°E), Indian mainland and adjacent oceans (IND, 10-25°N, 75-105°E), tropical Indian oceans (TIO, 10°S-10°N, 75-105°E), East Asian land (EA, 20-45°N, 105-123°E), and northwest Pacific Ocean (WNP, 5-20°N, 105-150°E), shown from the top left to the bottom right of Fig. 3.

Fig. 4a-e shows the quantitative estimation of the precipitation changes for the abovementioned regions in different experiments. In the STP (Fig. 4a), the mean precipitation is approximately 4.6 mm day^{-1} in the AMIP run, with a range from approximately 3.5 to 6.8 mm day^{-1}. This magnitude is quite similar to that in the CMIP run. When the topography is removed, the precipitation decreases to approximately 0.5 to 1.8 mm day^{-1} in A_NTP with a mean value of 1.1 mm day^{-1}, which accounts for 24.5% of the original precipitation in the AMIP run. The precipitation range in A_DIF is much larger than that in A_NTP. It ranges from 2 to 5.5 mm day^{-1} with a mean value close to 3.5 mm day^{-1}, which accounts for 75.5% of the original precipitation in the AMIP run. The above results denote that the model responses between the AMIP and CMIP runs are close to each other and that the TIP forcing is crucial for monsoon precipitation changes in the foothills of the southern TP.

In the Indian mainland and adjacent oceans (Fig. 4b), where the main branch of the SASM is located, the precipitation simulated in the AMIP run ranges from approximately 11 to 17 mm day^{-1}, with a mean value close to 14.5 mm day^{-1}. When the topography is removed, the simulated precipitation decreases in A_NTP, with a range from 6 to 14 mm day^{-1} and a mean value close to 10 mm day^{-1}, which accounts for almost 68.8% of the total precipitation in AMIP. The effects of the TIP thermodynamic forcing, which is denoted by A_DIF, show a precipitation range from 1 to 8 mm day^{-1}, with a mean value close to 4 mm day^{-1}, which accounts for 31.2% of the total precipitation in the AMIP run. The precipitation responses in the fully coupled model are quite similar to those in the atmosphereonly model, except that the simulated total precipitation in the CMIP run is slightly weaker than that in the AMIP run. These results suggest that the contributions of TIP forcing to the Indian mainland and adjacent oceans in the SASM region are approximately one-third of the total monsoon precipitation. It is also worth noting that the uncertainty in the precipitation response in A_DIF is considerably large. In the two extreme cases in A_DIF, the precipitation changes could either be 1 mm day^{-1} (7% of the total mean precipitation) or 8 mm day^{-1} (57% of the

total mean precipitation), which means that the TIP climate effect may be completely unimportant or relatively dominant in this region. The causes of this uncertainty and ways to reduce it are quite complex and worth further investigation.

The precipitation response in the TIO region is quite interesting (Fig. 4c). Unlike the SASM main branch, the total precipitation in the TIO region is quite small, with a mean value of 3 mm day^{-1} in the AMIP run and 4 mm day^{-1} in the CMIP run. However, the orographic forcing could induce a considerable impact on the precipitation changes in this region for both types of simulations. When the topography is removed, the precipitation simulated in A_NTP ranges from 3.2 to 5.8 mm day^{-1} with a mean value of 4.5 mm day^{-1}, which is approximately 142.8% of the total precipitation in the AMIP run. For the fully coupled run (C_NTP), the precipitation ranges from 3.5 to 6.8 mm day^{-1} with a mean value close to 5.2 mm day^{-1}, which is 131.6% of the total precipitation in the CMIP. The effect of TIP forcing causes the mean precipitation to decrease by 42.8% (A_DIF) and 31.6% (C_DIF) for the AMIP and CMIP runs, respectively. This result indicates that the remote TIP forcing could generally move the SASM rainbelt northward and reduce the precipitation in the TIO region by nearly one-third to half. However, we also need to pay attention to the uncertainty, which is denoted by the box length, as shown in A_DIF and C_DIF. It is clear that the model response could be more uncertain in the fully coupled run, with a maximum of 0.9 mm day^{-1} and a minimum of -4.5 mm day^{-1}.

For East Asian land (Fig. 4d), the precipitation simulated in the AMIP run ranges from 2.6 mm day^{-1} to 5.8 mm day^{-1} with a mean value of 4 mm day^{-1}. Surprisingly, when the topography is removed, the range of simulated precipitation in the A_NTP is even larger than that in the AMIP run, from 1.2 to 6.0 mm day^{-1}, with a mean of 3.2 mm day^{-1}, which accounts for 79.6% of the mean value in the AMIP run. Their differences (A_DIF) range widely in the model simulations, from -1.8 to 3.4 mm day^{-1}, with a mean value of 0.9 mm day^{-1}, which accounts for 20.4% of the mean value in the AMIP run. This result suggests that in most of the cases, the TIP effect on the changes in EASM precipitation is limited in the AMIP-type simulation, and in some extreme cases, the precipitation could even increase when the topography is removed. In contrast, the uncertainties in the fully coupled runs are smaller than those in the AMIP-type runs. Meanwhile, the mean precipitation in C_NTP is approximately 62.5% of that in the CMIP run, and the mean precipitation in C_DIF is approximately 37.5% of that in the CMIP run, which is higher than that in the AMIP type simulation. These results imply that air-sea interactions play an important role in the TIP climate effect over East Asia. This could reduce the uncertainty in the model response and amplify the TIP thermodynamic forcing on changes in the EASM.

The precipitation changes for the northwestern Pacific are shown in Fig. 4e. Because the surface is mainly covered by the ocean, convection is mainly triggered by changes in the SST. Therefore, in the AMIP-type runs, when the TIP topography is removed (A_NTP), the precipitation intensity remains almost unchanged, with a mean value close to 14 mm day^{-1}, which accounts for almost 97.3% of the precipitation in the AMIP run. The precipitation anomaly in most cases of A_DIF is close to 0 mm day^{-1}, while in some extreme cases, the precipitation anomaly is negative. In the fully coupled runs, the TIP effect on precipitation is

amplified. The mean precipitation in C_DIF could account for 23.1% of the mean precipitation in the CMIP run, while the maximum could achieve 5 mm day^{-1}, which is almost half of the mean precipitation in the CMIP run. This result highlights the important role of TIP thermodynamic forcing in modulating air-sea interactions and the associated monsoon system in the WNP region.

Based on the above analysis of the monsoon precipitation responses, we can conclude that the TIP thermodynamic forcing is a dominant trigger of monsoon precipitation on the southern slope of the TP. Moreover, the remote precipitation in the TIO is also quite sensitive to TIP forcing. In the East Asian land and WNP regions, the air-sea interaction plays an important role in amplifying the TIP forcing on changes in *in situ* monsoon precipitation. This result is qualitatively consistent with the study of Baldwin et al. [28], who found that the air-sea interaction is important for modulating TP forcing on the changes in precipitation over the Western Pacific by using the GFDL climate model. The key point is that tropical cyclones are well simulated in the control run [28]. Compared to a previous version of the FGOALS-s2 model results, which shows quite similar precipitation responses in the Western Pacific in both AGCM and CGCM, the control run of the model shows poor skill in capturing tropical cyclones over the Western Pacific [27]. Therefore, the improved simulation of tropical cyclones in a climate model will significantly affect the results of sensitive runs of orographic perturbation. Moreover, because the position of the western Pacific high is important for regulating the monsoon precipitation over East Asia and the WNP, we show the longitude of the west edge for the western Pacific high, which is denoted by the 1,485 gpm geopotential height contour in Fig. 4f. It is clear that in the AMIP and A_NTP runs, the positions of the western Pacific high are very close to each other, with a mean longitude of 147 °E. In contrast, the western Pacific high extends to 134 °E in the C_NTP but only extends to 145 °E in the CMIP. This result highlights that the influence of TIP forcing is crucial for regulating the western Pacific high through its influence on air-sea interactions.

3.3 Monsoon circulation and South Asian high responses

The South Asian monsoon and East Asian monsoon circulations are two important components in the Asian summer monsoon system. To quantitatively understand the responses of these two systems to TIP orographic forcing, three monsoon indices are adopted to describe the vertical and horizontal shear of the monsoon winds over South Asia and East Asia. The index defined by Webster and Yang (WYI) [57] considers the vertical wind shear over South Asia and covers the region of 5-20°N, 40-110°E. The South Asian monsoon is stronger when the vertical wind shear is stronger, which may be contributed by the enhancement of either the westerly at 850 hPa or the easterly at 200 hPa or both. Thus, a larger WYI value indicates a stronger South Asian monsoon.

In the AMIP run, the WYI is larger than 30 m s^{-1} for all cases, with a mean value close to 34 m s^{-1} and a range between 30 and 37 m s^{-1}. Compared to the AMIP run, the CMIP run shows a lower WYI, with a mean value of 26 m s^{-1}, which indicates that the simulated intensity of the South Asian monsoon is weaker in the CMIP run than in the AMIP run. This result is also consistent with the much stronger simulated South Asian monsoon precipitation

in the AMIP than in the CMIP runs (Fig. 3, a, d). The WYI responses are quite different in these two kinds of experiments. When the TIP orography is removed, the WYI is slightly weaker in A_NTP, with a mean WYI of 26 m s^{-1}, which is approximately 77.8% of the total intensity in the AMIP run. The mean WYI is only 7 m s^{-1} in A_DIF, with a range between almost 2 and 10 m s^{-1}. This result denotes that the influence of TIP thermodynamic forcing on the South Asian monsoon circulation is quite limited if the SST is prescribed in the model. However, the TIP heating effect could be amplified in the air-sea coupled run, and the mean WYI is approximately 12 m s^{-1} in C_DIF, which is approximately 43.2% of the WYI in the CMIP run.

There are many indices describing the EASM from various aspects [58]. In this paragraph, since we are mainly concerned with the low-level circulation changes in response to TIP forcing, we choose two indices that describe the horizontal shear of zonal and meridional winds. The first is the index defined by Wang and Fan [59]. They use the zonal wind differences at 850 hPa [U850 (5-15°N, 90-130°E) - U850 (22.5-32.5°N, 110-140°E)] as the monsoon index, here referred to as WF99. The other index is the meridional wind differences at 850 hPa [V850 (20-30°N, 110-140°E) - V850 (30-40°N, 110-140°E)], as defined in ref. [60], here referred to as WYF2001.

The WF99 index in different experiments is shown in Fig. 5b. The mean monsoon intensity is approximately 17 m s^{-1} in the AMIP run, with a range between approximately 9 and 22 m s^{-1}. When the TIP orography is removed, the monsoon intensity is nearly unaffected, as shown by the blue box (A_NTP). The mean monsoon response to TIP thermodynamic forcing is close to zero in A_DIF when nearly 25% of the simulations exhibit even negative index values, which means that in such cases, the zonal wind difference is even stronger when the orography is removed. However, when the air-sea interaction is considered, the zonal wind responses are different. The index in the CMIP run is overall weaker than that in the AMIP run, partly because the low-level monsoonal westerly flow is weaker (Fig. 3a, d). The mean intensity of the monsoon index decreases to 52.5% in C_NTP compared to that in the CMIP run, while the mean intensity is approximately 47.5% in C_DIF compared to that in the CMIP run. This result denotes that the TIP thermodynamic effect could contribute to nearly half of the low-level zonal wind difference of the EASM through the air-sea coupling process.

The WYF2001 indices simulated in the different experiments are shown in Fig. 5c. Compared to the zonal wind difference, the overall intensity of the meridional wind difference is quite weak. The mean intensities are approximately 0.25 m s^{-1} in the AMIP run and 0.26 m s^{-1} in the CMIP run, which are very close to each other. The TIP forcing is very limited in influencing the meridional wind difference of the EASM, and the mean difference of the WYF2001 in A_DIF accounts for only 17.6% of the original index in the AMIP run, while the mean difference of the WYF2001 in C_DIF accounts for 28.1% of the original index in the CMIP run. Moreover, the uncertainty of the TIP forcing on the changes in WYF2001 is also large. The intensity of the monsoon index ranges from -1 to 2.2 m s^{-1} in A_DIF and -1.8 to 1.9 m s^{-1} in C_DIF, which are even larger than those in the AMIP and CMIP runs. The above result implies that the effect of TIP thermodynamic forcing on the

low-level meridional wind changes is very unclear.

The South Asian High (SAH) is a prominent climate system in the upper troposphere over the Asian continent. The intensity and position of the SAH have great influences on East Asian weather and climate changes. The large-scale upper-level divergence of the SAH also contributes to the vertical wind shear over the Asian monsoon regions. Therefore, we evaluate the changes in SAH in different experiments and show the spatial distributions in Fig. 6. In the AMIP run (Fig. 6a), the 200 hPa geopotential height shows a clear close contour of 12,400 gpm, which covers the mid-latitude Asian continent and western Pacific Ocean. The intensity is much stronger than in the CMIP (Fig. 6d), which means that the SAH responses are quite sensitive to the SST simulation in the model. When the topography is removed in the A_NTP run (Fig. 6b), the SAH center is weakened and moves southeastward. The SAH responses in the C_NTP (Fig. 6e) are also quite similar to those in the A_NTP, and the SAH center moves southward to approximately 20 °N. The effect of TIP forcing on the SAH when the SST is prescribed (A_DIF) is shown in Fig. 6c. It is clear that an anticyclone anomaly accompanied by a positive geopotential height anomaly appears over the western TP at 200 hPa. However, when air-sea interactions are considered, the SAH responses to TIP forcing are stronger in C_DIF (Fig. 6f) than in A_DIF, which means that air-sea coupling could amplify the influence of TIP thermodynamic forcing on the upper-level circulation.

We aim to further quantitively understand the intensities and positions of the SAH responses to the TIP forcing in these experiments. Here, the intensity is calculated by averaging the SAH difference within the 0-40 °N, 20-160 °E box, and the difference is found to be above 20 gpm. We show the box plot of the SAH intensity for four kinds of experiments in Fig. 7a. The intensity of the SAH in the AMIP run is overall stronger than that in the CMIP run, but the difference is not as large as that shown in Fig. 6a and 6d. This result means that the systematic difference in mean geopotential height is large between the AMIP and CMIP runs, probably because the simulated SST in the CMIP run is colder than the observed SST and causes the atmosphere to be colder. When the TIP is removed in the model, the mean SAH intensity is reduced to 44 gpm in A_NTP, which accounts for 89.9% of the original intensity in the AMIP run. However, in C_NTP, the mean SAH intensity is reduced to 38 gpm, which accounts for 82.1% of the original intensity in the CMIP run. This result denotes that the air-sea interaction could amplify the influence of the TIP on the intensity of the SAH. The response of the SAH latitude is also similar to that of the intensity in these four experiments. Here, we define the mean SAH ridge latitude as the position where du/dy = 0. Fig. 7b shows that when air-sea coupling is considered in the model, the mean SAH ridge moves south to 18 °N, which is closer to the tropics than the result in A_NTP. All the above results indicate that the SAH is more sensitive to TIP thermodynamic forcing in the air-sea coupled simulation.

3.4 Regional mean meridional circulation responses

The remote effects of TIP thermodynamic forcing on tropical circulation have been addressed in previous studies [61-63]. Theoretically, the tropical atmospheric response to external forcing can develop a meridional circulation where the angular momentum

conservation (AMC) regime prevails [64-67]. Further analysis and numerical simulations [23] show that TIP thermal forcing plays an important role in producing meridional circulation from the Indian Ocean to the subtropical Asian continent. However, the previous numerical studies only show qualitative analysis. The relative role and a quantitative calculation of the TIP thermodynamic forcing on the changes in meridional circulation are unknown. In this section, the regional zonal mean meridional stream function (ZMPSI) [68] is calculated to quantitatively understand the TIP forcing effect on the changes in the regional zonal mean meridional circulation in the two types of simulations:

$$ZMPSI = \frac{2\pi R}{g}\int_{p}^{ps} v dp \qquad (7)$$

where v is the 60-120°E zonal mean meridional wind, p is pressure, ps is surface pressure, R is earth radius and g is the acceleration of gravity. Fig. 8a and 8d show the cross section of the 60-120°E JJA mean ZMPSI and the associated meridional wind vector in the AMIP and CMIP runs. The intensity of the ZMPSI in the AMIP is overall stronger than that in the CMIP, characterized by the center exceeding -3 $\times 10^{11}$ kg s^{-1}, which is located over 10°S-0. The meridional wind vectors mainly show a strong ascending branch over 10-20°N and a descending branch close to 20°S. Although the ZMPSI is weaker overall in the CMIP run (Fig. 8d), the negative ZMPSI (ascent motion) covers the subtropical Asian continent, which implies that the air-sea interaction could extend the meridional circulation simulation in the meridional direction.

The ZMPSI responses in the model when the TIP orography is removed are shown in Fig. 8b and 8e for A_NTP and C_NTP, respectively. The location of the main branch of the meridional circulation remains almost unchanged over the tropics. The largest difference is located over subtropical regions. The zero line of the ZMPSI shifts south to 20-40°N in A_NTP and C_NTP. Moreover, the simulated intensities of meridional circulation in the tropics are both weaker in these two experiments. These results suggest that TIP forcing enhances meridional circulation. To capture the vertical structure of the ZMPSI in response to TIP thermodynamic forcing, we show the cross sections of A_DIF and C_DIF in Fig. 8c and 8f, respectively. In A_DIF, the ZMPSI anomaly is strongly negative over the subtropics north of the TP and extends to the upper troposphere. The vectors mainly show ascending motion over the south slope of the TP with a local minimum of the ZMPSI anomaly in the middle troposphere. Moreover, the negative ZMPSI could extend to the tropics with the zero line over 10°S, which denotes the remote effects of TIP thermodynamic forcing. The ZMPSI anomaly in C_DIF (Fig. 8f) is basically similar to that in A_DIF, except the intensity is slightly weaker.

In comparing Fig. 8b and 8c as well as Figs. 8e and 8f, the relative importance of TIP forcing on the changes in ZMPSI differs from the tropics to subtropics. We further calculate the regional mean ZMPSI for two latitude bands to quantitively understand the TIP forcing on changes in the regional ZMPSI. The first is the 10°S-10°N mean ZMPSI (Fig. 9a). The mean ZMPSI for the AMIP run is approximately -3.9×10^{11} kg s^{-1}, with a range from -3.1×10^{11} kg s^{-1} to -4.5×10^{11} kg s^{-1}. When the TIP orography is removed, the mean ZMPSI in A_NTP increases to approximately -3.4×10^{11} kg s^{-1}, which is comparable to the ZMPSI in the AMIP

run. Therefore, the mean ZMPSI in A_DIF is only – 0.6×10^{11} kg s^{-1}, which is equivalent to 14.6% of the ZMPSI intensity in the AMIP run. The mean ZMPSI is approximately -3.2×10^{11} kg s^{-1} in the CMIP run and -2.4×10^{11} kg s^{-1} in the C_NTP run. The associated mean ZMPSI is -0.8×10^{11} kg s^{-1} in C_DIF, which is equivalent to 23% of the ZMPSI intensity in the CMIP run. These results indicate that the remote influences of the TIP on the topical meridional circulation are limited even when air-sea interactions are considered in the model. The other latitude band is 10-30°N for the subtropical region. We show the calculated ZMPSI in Fig. 9b. The mean ZMPSI is approximately -1.4×10^{11} kg s^{-1} in the AMIP run and approximately -0.4×10^{11} kg s^{-1} in A_NTP. Therefore, the associated ZMPSI difference is approximately -1 kg s^{-1} in A_DIF. This is equivalent to almost 70% of the mean ZMPSI in the AMIP run. For the coupled run, the mean ZMPSI is approximately -1.3×10^{11} kg s^{-1} in the CMIP run and -0.7×10^{11} kg s^{-1} in C_NTP, while the mean ZMPSI difference is approximately -0.6×10^{11} kg s^{-1} in C_DIF, which is equivalent to 46.9% of the ZMPSI intensity in the CMIP run. The above results indicate that the TIP thermodynamic forcing is crucial for producing meridional circulation from the Indian Ocean to the Asian continent during boreal summer, and the air-sea interaction will weaken the TIP influence on the circulation compared to that in the AMIP simulation.

4. Conclusion and discussion

In this study, the SPV is calculated and used to evaluate the thermodynamic forcing changes in the FGOALS-f2 climate model when the TIP orography is removed in the AMIP and CMIP simulations. The responses of the Asian summer monsoon system to orographic changes are quantitively evaluated and summarized in Table 2.

First, the SPV responses are quite different in A_NTP and C_NTP, although the same topography is removed. The mean SPV is reduced to almost zero in A_NTP, while it is only reduced to 32% of the SPV in the CMIP run for C_NTP. The air-sea interaction compensates for the thermal forcing changes over the Asian continent in the coupled model. Since the dynamic effect of TIP is completely removed in these experiments, the SPV differences mainly originate from the thermal forcing changes when the topography is modified for different model configurations. These SPV differences could lead to different ASM responses in the model.

Second, quantitative evaluations of the precipitation for different regions of the ASM in response to the TIP thermodynamic forcing are summarized here. The precipitation response over the southern slope of the TP is most sensitive to the changes in orography, which equals 75.5% for A_DIF/AMIP and 73.6% for C_DIF/CMIP. For the other regions, although the influences of TIP forcing on the precipitation changes are not dominant, the quantitative precipitation responses are not small and cannot be neglected. In particular, for the tropical Indian Ocean, the changes in precipitation are negative in response to perturbed orography. Moreover, for the northwestern Pacific Ocean, the influence of the TIP in A_DIF is very limited, but it accounts for 23.1% in C_DIF/CMIP, which indicates the importance of air-sea interactions in adjusting the TIP thermodynamic forcing on the ASM.

Third, the responses of ASM circulations and associated climate systems, such as the

South Asian High and Western Pacific High, are also quite different in these two kinds of experiments. The vertical shear of the winds in the SASM regions denoted by the WYI increases by 22.2% with the presence of the TIP in the AMIP run, while it increases by 43.2% in the CMIP run. The responses of the horizontal wind shear over EASM regions are quite limited in the AMIP run and are more sensitive in the CMIP run. For the meridional circulation, the response of regional meridional circulation near the tropics is relatively small, while in the subtropics (10-30°N), the response is more sensitive in the AMIP run, with an increase ratio of 70.0%, and less sensitive in the CMIP run. The SAH is intensified along the subtropical high ridge to the west with the presence of the TIP, while the WPH could extend westward when the TIP is removed in the coupled model.

Notably, the TP-SPV changes are quite different between the A_DIF and C_DIF, while the air-sea interaction plays an important role in adjusting the TIP thermodynamic forcing when the topography is removed in the model. Therefore, the thermodynamic forcing of the TIP may be less sensitive in the coupled model since the TP-SPV changes are weaker than those in the AMIP run. To have a visual impression of the precipitation changes relative to the TP-SPV changes in the two types of experiments, we show a map of the relative ratio of the monsoon precipitation percentage changes to TP-SPV percentage changes in Fig. 10. The ratios are calculated by the percentage changes in precipitation for the five regions, as shown in Table 2, divided by the TP-SPV in the first row for both the AMIP and CMIP experiments. The larger the ratio is, the more sensitive the precipitation changes to the TP-SPV changes. The standard deviations are shown as the yellow numbers under each box; the larger the standard deviation is, the more uncertain the precipitation responses. It is clear that the precipitation response is stronger overall in the CMIP type runs and is the largest over the south slope of the TP. Moreover, the model responses in the WNP, Indian mainland and northern Indian Ocean exhibit the highest uncertainties.

Notably, although we show the quantitative relationship between the TIP thermodynamic forcing and the ASM circulation and precipitation in the FGOALS-f2 model for the AMIP and CMIP experiments, the systematic model bias in capturing the observed monsoon system will certainly influence the accuracy estimations of the interaction between the TIP and ASM in the model [see Online supplemental material (OSM) for details]. For example, as documented in Fig. S4 in OSM and Section 3.2 in this study, the AMIP simulation mainly overestimates the precipitation over the northern Indian Ocean and underestimates the precipitation over Asian land, especially over East Asia. Therefore, in the sensitivity experiments when the TIP topography is removed, the precipitation response over East Asian land may be underestimated, and the response over the northern Indian Ocean may be overestimated. Additionally, both the AMIP and CMIP runs underestimate the SPV over the TP (Fig. S2 in OSM), which may lead to negative precipitation biases over Asian land regions (Fig. S4 in OSM). The possible cause and effect relationships need future studies. From this perspective, the quantitative calculation of the monsoon response in this study is mainly used for measuring the model behavior between the AMIP and CMIP runs. The results can serve as a reference for understanding the role of air-sea interactions in adjusting the model response to TIP orographic forcing and for further model development and

performance optimization.

Another way to reduce the uncertainty of the calculated TIP thermodynamic forcing effects on the ASM is to use state-of-the-art multimodel ensembles. As documented in Tebaldi and Knutti [69], the multimodel ensemble is an effective method for reducing individual model biases, which may originate from either the initial conditions or the dynamic and physical parameterization of the model. Usually, the multimodel mean (MME) is better at capturing the observation features. Sperber et al. [70] analyzed 25 CMIP5 and 22 CMIP3 model simulations to capture the spatial and temporal features of the ASM. They indicated that no single model best represents all of the aspects of the monsoon, but the CMIP5 MME is better skilled than the CMIP3 according to all the diagnostics used to test their monsoon pattern simulation skills. Therefore, to better understand the role of the TIP on the simulations of the ASM and to reduce model bias in the dynamic core and physical parameterization associated with the TIP topography, it is necessary to examine MME responses to orographic perturbation experiments and to test the influences among different resolutions and model physics in the future. These approaches will advance the study of Tibetan Plateau orographic forcing and Asian monsoon dynamics.

Declaration of competing interest

The authors declare that they have no conflicts of interest in this work.

Acknowledgments

We would like to thank the three anonymous reviewers for their constructive suggestions, which helped to improve the overall quality of the manuscript. The research presented in this paper is jointly funded by the National Natural Science Foundation of China (42122035, 42288101, and 91937302) and the Guangdong Major Project of Basic and Applied Basic Research (2020B0301030004).

References

[1] J. G. Charney, On a physical basis for numerical prediction of large-scale motions in the atmosphere, J. Atmos. Sci. 6 (1949) 372-385.

[2] J. G. Charney, A. Eliassen, A numerical method for predicting the perturbations of the middle latitude westerlies, Tellus 1 (1949) 38-54.

[3] P. Queney, The problem of air flow over mountains: A summary of theoretical studies, Bull. Amer. Meteor. Soc. 29 (1948) 16-29.

[4] B. Bolin, On the influence of the earth's orography on the general character of the westerlies, Tellus 2 (1950) 184-195.

[5] T. C. Yeh, The circulation of the high troposphere over China in the winter of 1945-1946, Tellus 2 (1950) 173-183.

[6] D. G. Hahn, S. Manabe, The role of mountains in the South Asian monsoon circulation, J. Atmos. Sci. 32 (1975) 1515-1541.

[7] G. X. Wu, W. P. Li, H. Guo, et al., Sensible heat driven air-pump over the Tibetan Plateau and its impacts on the Asian summer monsoon, In: Ye, DZ (ed.), Collections on the Memory of Zhao Jiuzhang, Science Press, Beijing, 1997, pp. 116-26. (in Chinese).

[8] G. X. Wu, Y. M. Liu, Q. Zhang, et al., The influence of the mechanical and thermal forcing of the Tibetan Plateau on the Asian climate, J. Hydrometeorol. 8 (2007) 770-789.

[9] W. L. Gates, AMIP: The atmospheric model intercomparison project, Bull. Amer. Meteor. Soc. 73 (1992) 1962-1970.

[10] G. A. Meehl, G. J. Boer, C. Covey, et al., Intercomparison makes for a better climate model, Eos, Tran. Amer. Geo. Union 78 (1997) 445-451.

[11] G. A. Meehl, G. J. Boer, C. Covey, et al., The Coupled Model Intercomparison Project (CMIP), Bull. Amer. Meteor. Soc. 81 (2000) 313-318.

[12] W. C. Chao, B. Chen, The origin of monsoons, J. Atmos. Sci. 58 (2001) 3497-3507.

[13] X. D. Liu, Z. Y. Yin, Sensitivity of East Asian monsoon climate to the uplift of the Tibetan Plateau, Palaeogeo. Palaeocli. Palaeoeco. 183 (2002), 223-245.

[14] M. Abe, A. Kitoh, T. Yasunari, An evolution of the Asian summer monsoon associated with mountain uplift-simulation with the MRI atmosphere-ocean coupled GCM, J. Meteorol. Soc. Jpn. 81 (2003) 909-933.

[15] A. Kitoh, Effects of mountain uplift on East Asian summer climate investigated by a coupled atmosphere-ocean GCM, J. Clim. 17 (2004) 783-802.

[16] A. Kitoh, T. Motoi, O. Arakawa, Climate modeling study on mountain uplift and Asian monsoon evolution, Geo. Soc. Spe. Pub. 342 (2010) 293-301.

[17] H. Okajima, S. P. Xie, Orographic effects on the northwestern Pacific monsoon: Role of air-sea interaction, Geophy. Res. Lett. 34 (1997) L21708.

[18] S. Koseki, M. Watanabe, M. Kimoto, Role of the midlatitude air-sea interaction in orographically forced climate, J. Meteorol. Soc. Jpn. 86 (2008) 335-351.

[19] Z. F. Xu, C. B. Fu, Y. F. Qian, Relative roles of land-sea distribution and orography in Asian monsoon intensity, J. Atmos. Sci. 66 (2009) 2714-2729.

[20] W. R. Boos, Z. Kuang, Dominant control of the South Asian monsoon by orographic insulation versus plateau heating, Nature 463 (2010) 218-222.

[21] Z. F. Xu, Y. F. Qian, C. B. Fu, The role of land-sea distribution and orography in the Asian monsoon. Part II: Orography, Adv. Atmos. Sci. 27 (2010) 528-542.

[22] H. S. Park, J. C. H. Chiang, S. Bordoni, The mechanical impact of the Tibetan Plateau on the Seasonal Evolution of the South Asian Monsoon, J. Clim. 25 (2012) 2394-2407.

[23] G. X. Wu, Y. M. Liu, B. He, et al., Thermal controls on the Asian summer monsoon, Sci. Rep. 2 (2012) 404.

[24] G. S. Chen, Z. Liu, J. E. Kutzbach, Reexamining the barrier effect of the Tibetan Plateau on the South Asian summer monsoon, Clim. Past 10 (2014) 1269-1275.

[25] B. He, G. X. Wu, Y. M. Liu, et al., Astronomical and hydrological perspective of mountain impacts on the Asian summer monsoon, Sci. Rep. 5 (2015) 17586.

[26] B. He, Q. Bao, X. C. Wang, et al., CAS FGOALS-f3-L model datasets for CMIP6 historical Atmospheric Model Intercomparison Project simulation, Adv. Atmos. Sci. 36 (2019) 771–778.

[27] B. He, Y. M. Liu, G. X. Wu, et al., The role of air–sea interactions in regulating the thermal effect of the Tibetan-Iranian Plateau on the Asian summer monsoon, Clim. Dyn. 52 (2019) 4227-4245.

[28] J. W. Baldwin, G. A.Vecchi, S. Bordoni, The direct and ocean-mediated influence of Asian orography on tropical precipitation and cyclones, Clim. Dyn. 53 (2019) 805-824.

[29] J. H. Son, K. H. Seo, B. Wang, Dynamical control of the Tibetan Plateau on the East Asian summer monsoon, Geophy. Res. Lett. 46 (2019) 7672-7679.

[30] R. P. Acosta, M. Huber, Competing topographic mechanisms for the summer Indo-Asian monsoon, Geophy. Res. Lett. 47 (2020) e2019GL085112.

[31] M. Ashfaq, Topographic controls on the distribution of summer monsoon precipitation over South Asia, Earth Syst. Environ. 4 (2020) 667-683.

[32] B. He, Influences of elevated heating effect by the Himalaya on the changes in Asian summer monsoon, Theor. Appl. Climatol. 128 (2017) 905-917.

[33] W. R. Boos, Z. Kuang, Sensitivity of the South Asian monsoon to elevated and non-elevated heating, Sci. Rep. 3 (2013) 1192.

[34] Z. Q. Wang, A. M. Duan, S. Yang, Potential regulation on the climatic effect of Tibetan Plateau heating by tropical air–sea coupling in regional models, Clim. Dyn. 52 (2018) 1685-1694.

[35] D. Ma, W. Boos, Z. Kuang, Effects of orography and surface heat fluxes on the south asian summer monsoon, J. Clim. 27 (2014) 6647–6659.

[36] M.M. Lu, S. Yang, J. B. Wang, et al., Response of regional asian summer monsoons to the effect of reduced surface albedo in different tibetan plateau domains in idealized model experiments, J. Clim. (2021) 1-49.

[37] B. He, C. Sheng, G. X. Wu, et al., Quantification of seasonal and interannual variations of the Tibetan Plateau surface thermodynamic forcing based on the potential vorticity, Geophy. Res. Lett. 49 (2022) e2021GL097222.

[38] L. J. Zhou, Q. Bao, Y. M. Liu, et al., Global energy and water balance: Characteristics from Finite-volume Atmospheric Model of the IAP/LASG (FAMIL1), J. Adv. Model. Earth Syst. 7 (2015) 1-20.

[39] Q. Bao, X. F. Wu, J. X. Li, et al., Outlook for El Nino and the Indian Ocean Dipole in autumn-winter 2018–2019 (in Chinese), Chin. Sci. Bull. 64 (2018) 73-78.

[40] J. X. Li, Q. Bao, Y. M. Liu, et al., Evaluation of FAMIL2 in simulating the climatology and seasonal-to-interannual variability of tropical cyclone characteristics, J. Adv. Model. Earth Syst. 11 (2019) 1117-1136.

[41] D. J. Kerbyson, P. W. Jones, A performance model of the parallel ocean program, Inter. J. High Perfor. Compu. Appl. 19 (2005) 261-276.

[42] K. W. Oleson, D. M. Lawrence, G. B. Bonan, et al., Technical description of version 4.0 of the Community Land Model (CLM), NCAR technical note , NCAR, 2010, pp. 173.

[43] E. C. Hunke, W. H. Lipscomb, A. K. Turner, et al., CICE: the Los Alamos Sea Ice Model Documentation and Software User's Manual Version 4.1, T-3 Fluid Dynamics Group, Los Alamos National Laboratory, 2010, pp. 675.

[44] S. J. Lin, A "vertically Lagrangian" finite-volume dynamical core for global models, Mon. Wea. Rev. 132 (2004) 2293-2307.

[45] W. M. Putman, S. J. Lin, Finite-volume transport on various cubed-sphere grids, J. Comput. Phys. 227 (2007) 55-78.

[46] C. S. Bretherton, S. Park, A new moist turbulence parameterization in the Community Atmosphere Model, J. Climate 22 (2009) 3422-3448.

[47] X. Wang, M. Zhang, Vertical velocity in shallow convection for different plume types, J. Adv. Model. Earth Syst. 6 (2014) 478-489.

[48] Y. L. Lin, R. D. Farley, H. D. Orville, Bulk parameterization of the snow field in a cloud model, J. Clim. Appl. Meteorol. 22 (1983) 1065-1092.

[49] L. M. Harris, S. J. Lin, Global-to-regional nested grid climate simulations in the GFDL high resolution atmospheric model, J. Clim. 27 (2014) 4890-4910.

[50] K. M. Xu, D. A. Randall, A semiempirical cloudiness parameterization for use in climate models, J. Atmos. Sci. 53 (1996) 3084-3102.

[51] S. A. Clough, M. W. Shephard, E. J. Mlawer, et al., Atmospheric radiative transfer modeling: A summary of the AER codes, J. Quant. Spectrosc. Radiat. Transfer 91 (2005) 233–244.

[52] T. N. Palmer, G. J. Shutts, R. Swinbank, Alleviation of a systematic westerly bias in general circulation and numerical weather prediction models through an orographic gravity wave drag parametrization, Quart. J. Roy. Meteor. Soc. 112 (1986) 1001-1039.

[53] V. Eyring, S. Bony, G. A. Meehl, et al., Overview of the Coupled Model Intercomparison Project Phase 6 (CMIP6) experimental design and organization, Geosci. Model Dev. 9

(2016) 1937-1958.

[54] B. He, Y. M. Liu, G. X. Wu, et al., CAS FGOALS-f3-L model datasets for CMIP6 GMMIP Tier-1 and Tier-3 experiments, Adv. Atmos. Sci. 37 (2020) 18-28.

[55] B. He, Y. Q. Yu, Q. Bao, et al., CAS FGOALS-f3-L model dataset descriptions for CMIP6 DECK experiments, Atmos. Ocea. Sci. Lett. 13 (2020) 576-581.

[56] Y. J. Song, X. F. Li, Y. Bao, et al., FIO-ESM v2.0 outputs for the CMIP6 Global Monsoons Model Intercomparison Project experiments, Adv. Atmos. Sci. 37 (2020) 1045-1056.

[57] P. J. Webster, S. Yang, Monsoon and ENSO: Selectively interactive systems, Quart. J. Roy. Meteor. Soc. 118 (1992) 877-926.

[58] B. Wang, Z.W. Wu, J.P. Li, et al., How to measure the strength of the East Asian summer monsoon, Journal of Climate 21 (2008) 4449-4463.

[59] B. Wang, Z. Fan, Choice of South Asian summer monsoon indices, Bull. Amer. Meteor. Soc. 80 (1999) 629-638.

[60] Y. Wang, B. Wang, J. H. Oh, Impact of the preceding ElNiño on the east Asian summer atmosphere circulation, J. Meteorol. Soc. Jpn. 79 (2001) 575-588.

[61] G. X. Wu, A. M. Duan, Y. M. Liu, et al., Tibetan Plateau climate dynamics: recent research progress and outlook, Nat. Sci. Rev. 2 (2015) 100-116.

[62] G. X. Wu, B. He, Y. M. Liu, et al., Location and variation of the summertime upper-troposphere temperature maximum over South Asia, Clim. Dyn. 45 (2015) 2757-2774.

[63] Y. M. Liu, M.M. Lu, H.J. Yang, et al., Land–atmosphere–ocean coupling associated with the Tibetan Plateau and its climate impacts, Nat. Sci. Rev. 7 (2020) 534-552.

[64] E. K. Schneider, Axially symmetric steady-state models of the basic state for instability and climate studies. Part II. Nonlinear calculations, J. Atmos. Sci. 34 (1977) 280-296.

[65] E. K. Schneider, R. S. Lindzen, Axially symmetric steady-state models of the basic state for instability and cli- mate studies. Part I. Linearized calculations, J. Atmos. Sci. 34 (1977) 263–279.

[66] E. K. Schneider, A simplified model of the modified Hadley circulation, J. Atmos. Sci. 44 (1987) 3311–3328.

[67] I. M. Held, A. Y. Hou, Nonlinear axially symmetric circulations in a nearly inviscid atmosphere, J. Atmos. Sci. 37 (1980) 515–533.

[68] L. E. Buja, CCM Processor User's Guide (Unicos Version), NCAR Technical Note, NCAR, 1994, pp. B-17-18.

[69] C. Tebaldi, R. Knutti, The use of the multi-model ensemble in probabilistic climate projections, Philo. Trans. Royal Soc. A. Mathematical. Phys. Eng. Sci. 365 (2007) 2053–2075.

[70] K. R. Sperber, H. Annamalai, I. S. Kang, et al., The Asian summer monsoon: an intercomparison of CMIP5 vs. CMIP3 simulations of the late 20th century, Clim. Dyn. 41

(2013) 2711–2744.

Figures and Tables

Table 1. Experimental design. In AMIP and A_NTP, the model is forced by the observed SST and sea ice. The model integrated from 1970 to 2014, when the first 9 years are recognized as spin-up time, and the period from 1979 to 2014 is used for analysis, i.e., 36 samples are available for the statistical analysis. In CMIP and C_NTP. The model ran 500 years for the spin-up period with full topography, then the model additionally ran for 100 years (without topography in C_NTP), and the last 50 years (50 samples) were used here for analysis. More detailed descriptions are provided in Section 2.2.

Experiment	Topography	Air-sea coupling
AMIP	Full	No
A_NTP	No Tibetan and Iranian Plateau	No
CMIP	Full	Yes
C_NTP	No Tibetan and Iranian Plateau	Yes

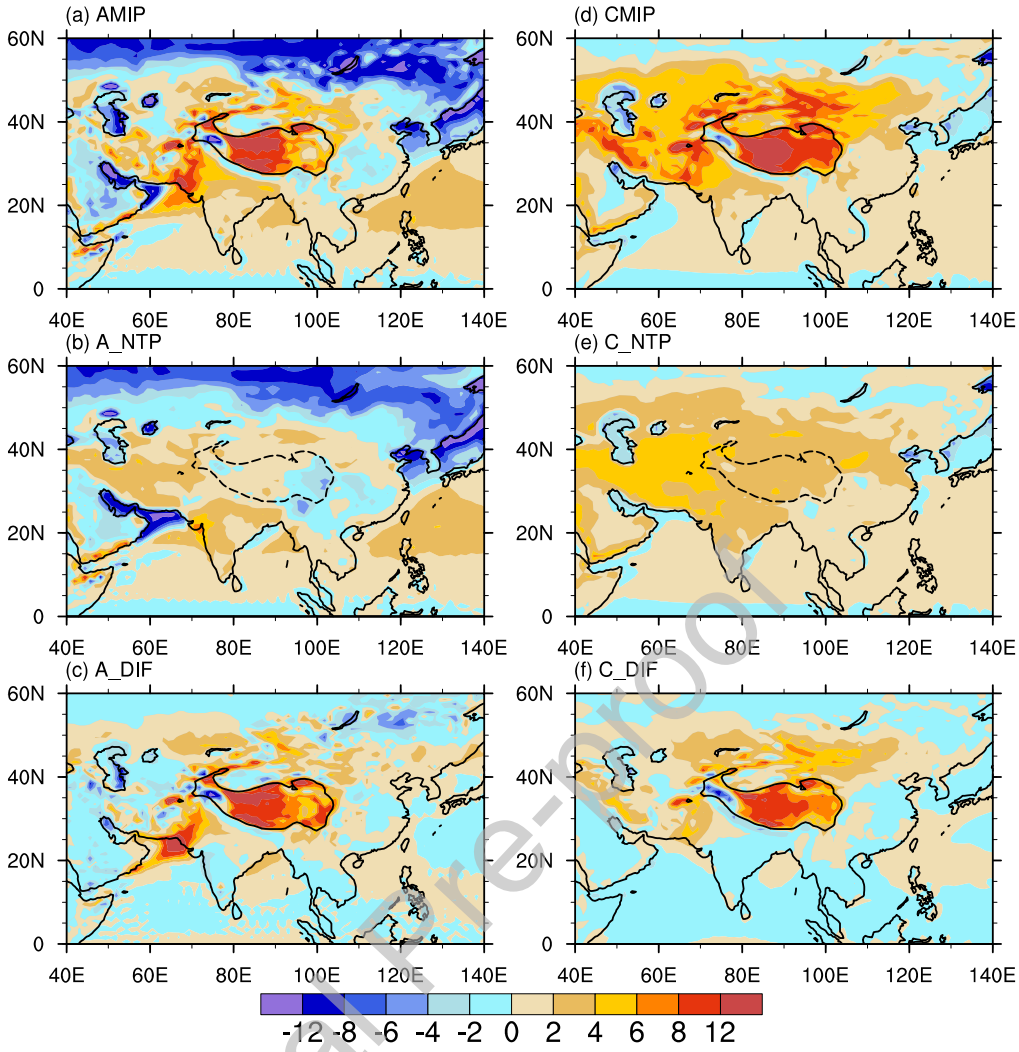

Fig. 1. Climate mean of the JJA SPV (PVU, 1 PVU = 10^{-6} K m^2 kg^{-1} s^{-1}) in different experiments: (a) AMIP, (b) A_NTP, (c) A_DIF, (d) CMIP, (e) C_NTP, and (f) C_DIF. The solid and dashed lines denote the topography above 3,000 m.

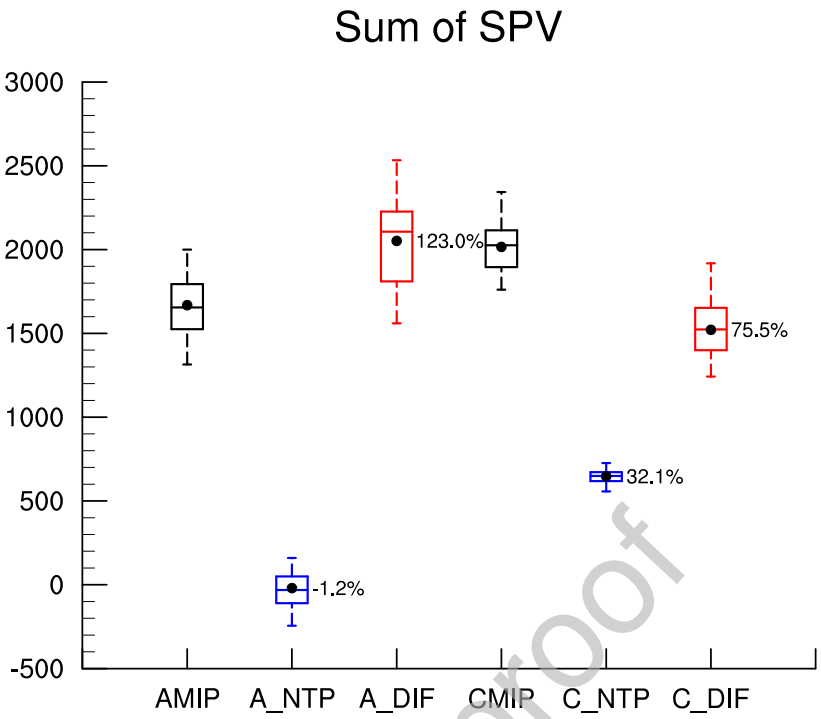

Fig. 2. Boxplot for the regional sum of SPV (PVU, 1 PVU = 10^{-6} K m^2 kg^{-1} s^{-1}) above 3000 m of the AMIP topography for the different experiments. The black dots denote the mean value of the datasets, and the percentages denote the mean value of the A_NTP (or A_DIF) divided by AMIP runs, and the mean value of the C_NTP (or C_DIF) divided by CMIP runs.

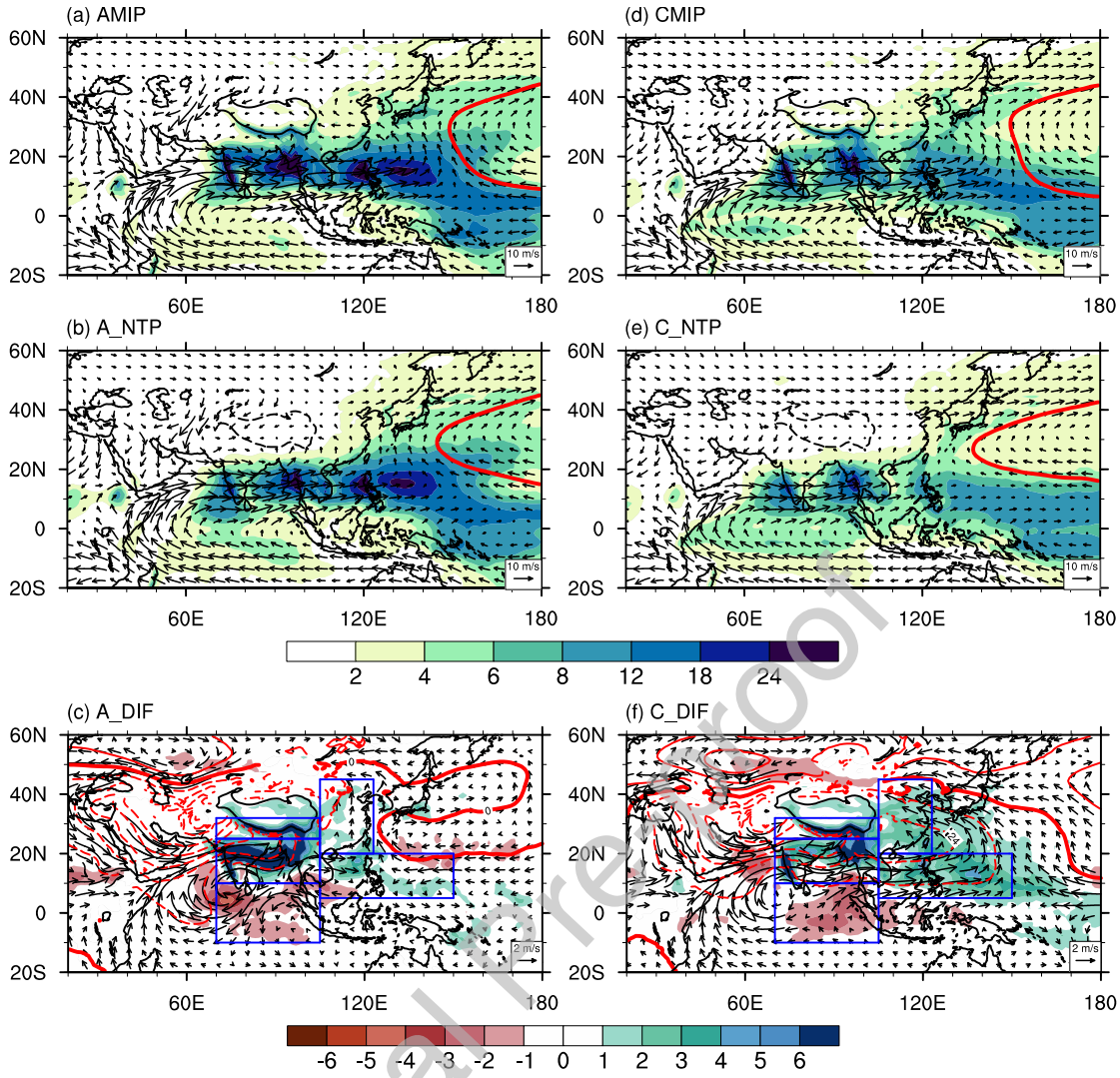

Fig. 3. Climate mean of the JJA precipitation (shading, mm day^{-1}) and 850 hPa winds (m s^{-1}) for (a) AMIP, (b) A_NTP, (c) A_DIF, (d) CMIP, (e) C_NTP, and (f) C_DIF. The red contour in (a, b, d, e) denotes the 1,485 geopotential height (gpm) at 850 hPa. The red contours in (c, f) are the geopotential height differences (gpm) at 850 hPa. The blue boxes denote the regions of the south Tibetan Plateau (25-32°N, 75-105°E), Indian mainland and adjacent oceans (10-25°N, 75-105°E), tropical Indian oceans (10°S-10°N, 75-105°E), East Asian land (20-45°N, 105-123°E), and northwest Pacific ocean (5-20°N, 105-150°E), from the top left to the bottom right. The solid and dashed black lines denote the topography above 3,000 m.

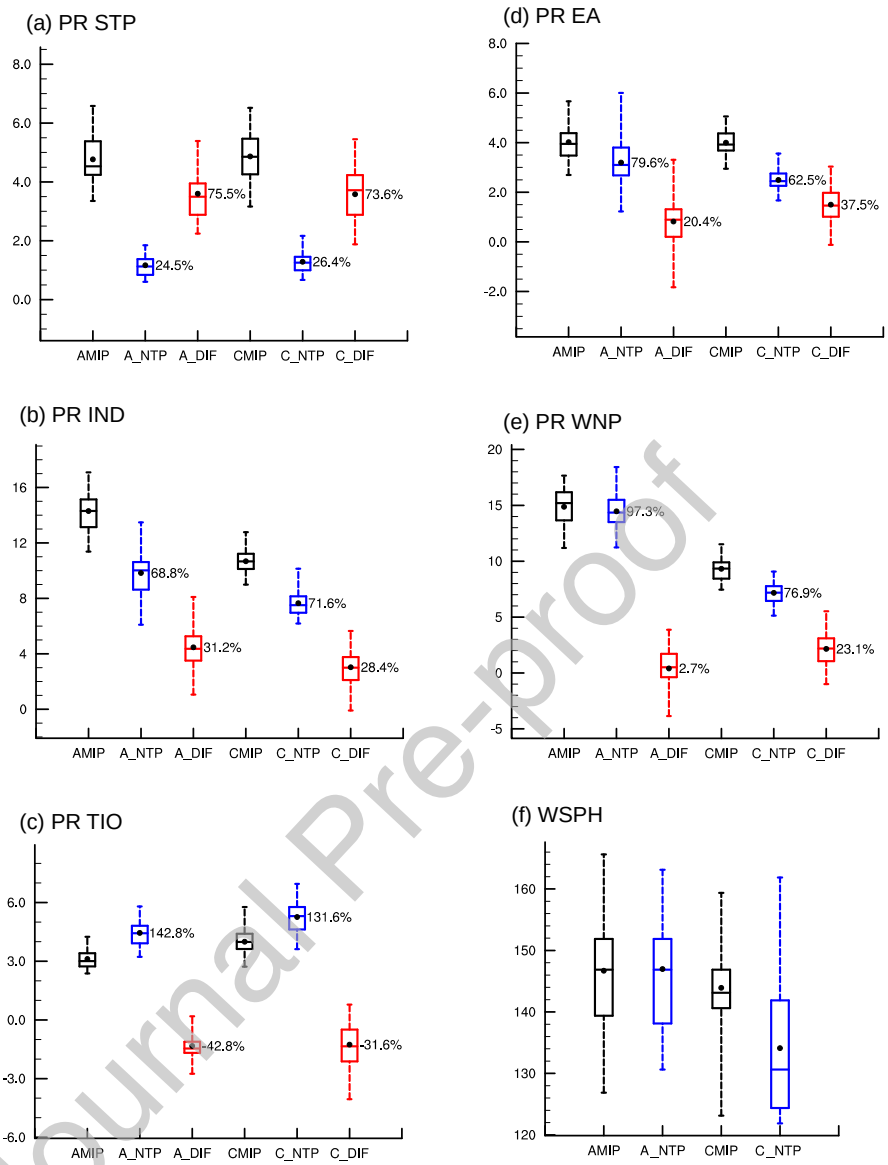

Fig. 4. Boxplot of the regional mean JJA precipitation (mm day^{-1}) and longitude of the west point for the simulated western Pacific high in the different experiments. The black dots denote the mean values of the datasets, and the percentages denote the mean value of the A_NTP (or A_DIF) divided by AMIP runs, and the mean value of the C_NTP (or C_DIF) divided by CMIP runs. (a) Precipitation on the southern Tibetan Plateau (25-32°N, 75-105°E), (b) precipitation on the Indian mainland and over its adjacent oceans (10-25°N, 75-105°E), (c) precipitation over the tropical Indian oceans (10°S-10°N, 75-105°E), (d) precipitation on East Asian land (20-45°N, 105-123°E), (e) precipitation over the northwest Pacific Ocean (5-20°N, 105-150°E), and (f) the longitude of the west edge for the western Pacific high denoted by the 1,485 gpm geopotential height contour at 850 hPa.

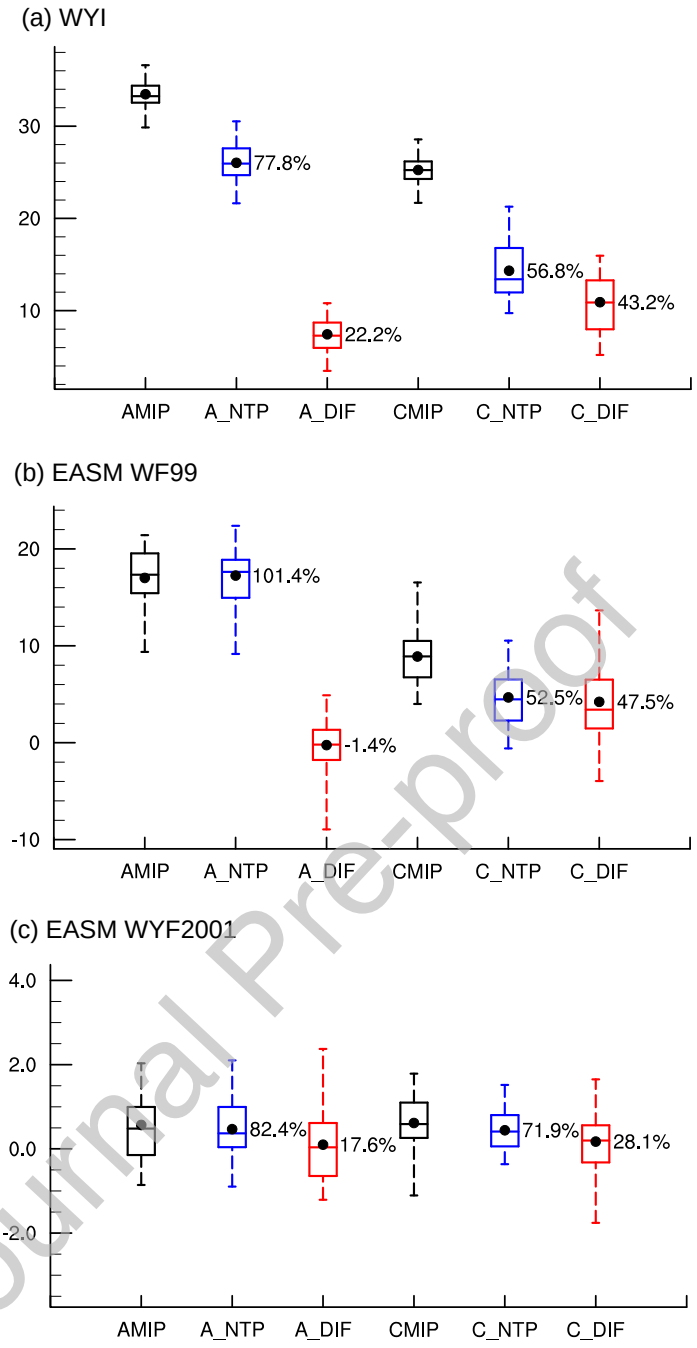

Fig. 5. Boxplot of the (a) South Asian summer monsoon index in the different experiments, which is the vertical zonal wind shear (U850-U200, 5-20°N, 40-110°E) as defined by Webster and Yang (1992); (b) East Asian summer monsoon index in the different experiments, which is the zonal wind difference at 850 hPa [U850 (5-15°N, 90-130°–) - U850 (22.5-32.5°N, 110-140°E)] as defined in Wang and Fan (1999); and (c) East Asian summer monsoon index in the different experiments, which is the meridional wind difference at 850 hPa [V850 (20-30°N, 110-140°E) - V850 (30-40°N, 110-140°E)] as defined in Wang et al. (2001). The black dots denote the mean value of the datasets, and the percentages denote the mean value of the A_NTP (or A_DIF) divided by AMIP runs, and the mean value of the C_NTP (or C_DIF) divided by CMIP runs.

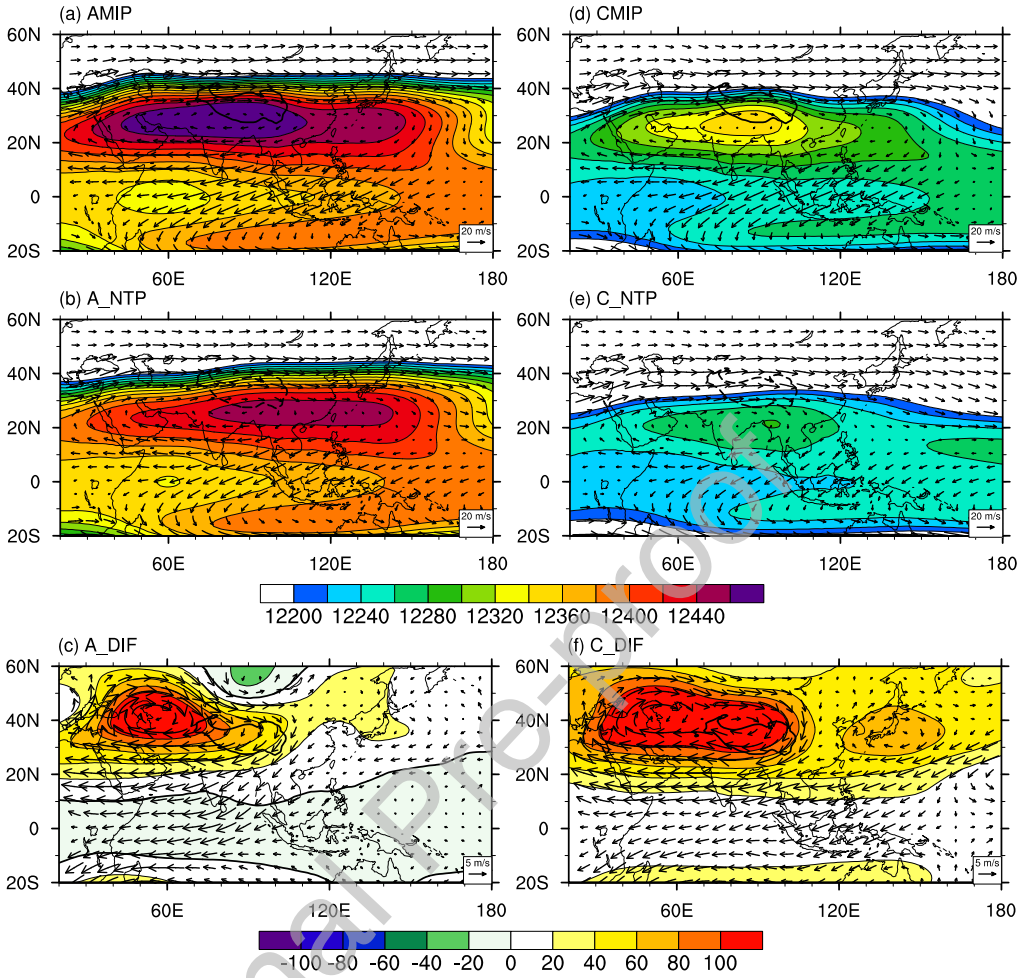

Fig. 6. Climate mean of the JJA 200 hPa geopotential height (shaded, gpm) and winds (vectors, m s^{-1}) in different experiments: (a) AMIP, (b) A_NTP, (c) A_DIF, (d) CMIP, C_NTP, and (f) C_DIF. The solid and dashed black lines denote the topography above 3,000 m.

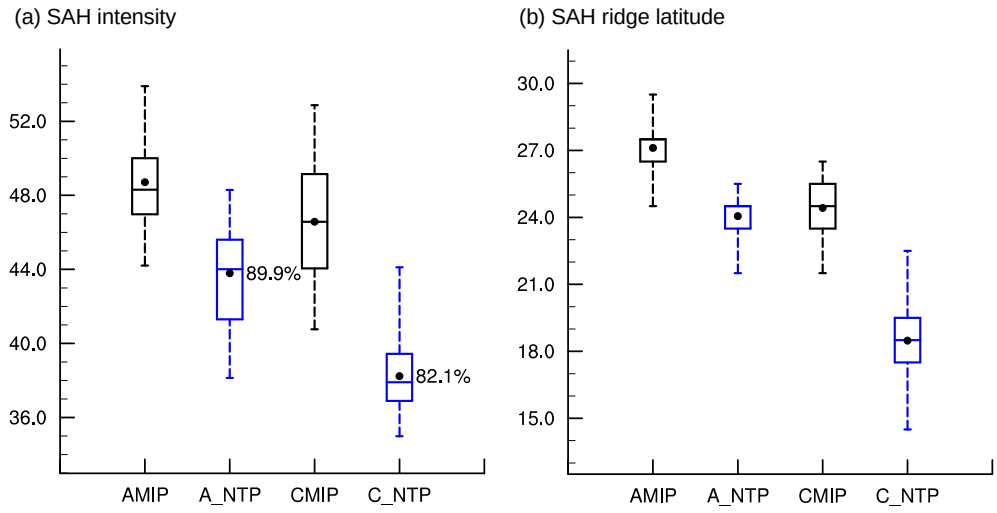

Fig. 7. Boxplot of the (a) South Asian High intensity and (b) the latitude of the South Asian High ridge. The black dots denote the mean value of the datasets, and the percentages denote the mean value of the A_NTP divided by AMIP runs, and the mean value of the C_NTP divided by CMIP runs.

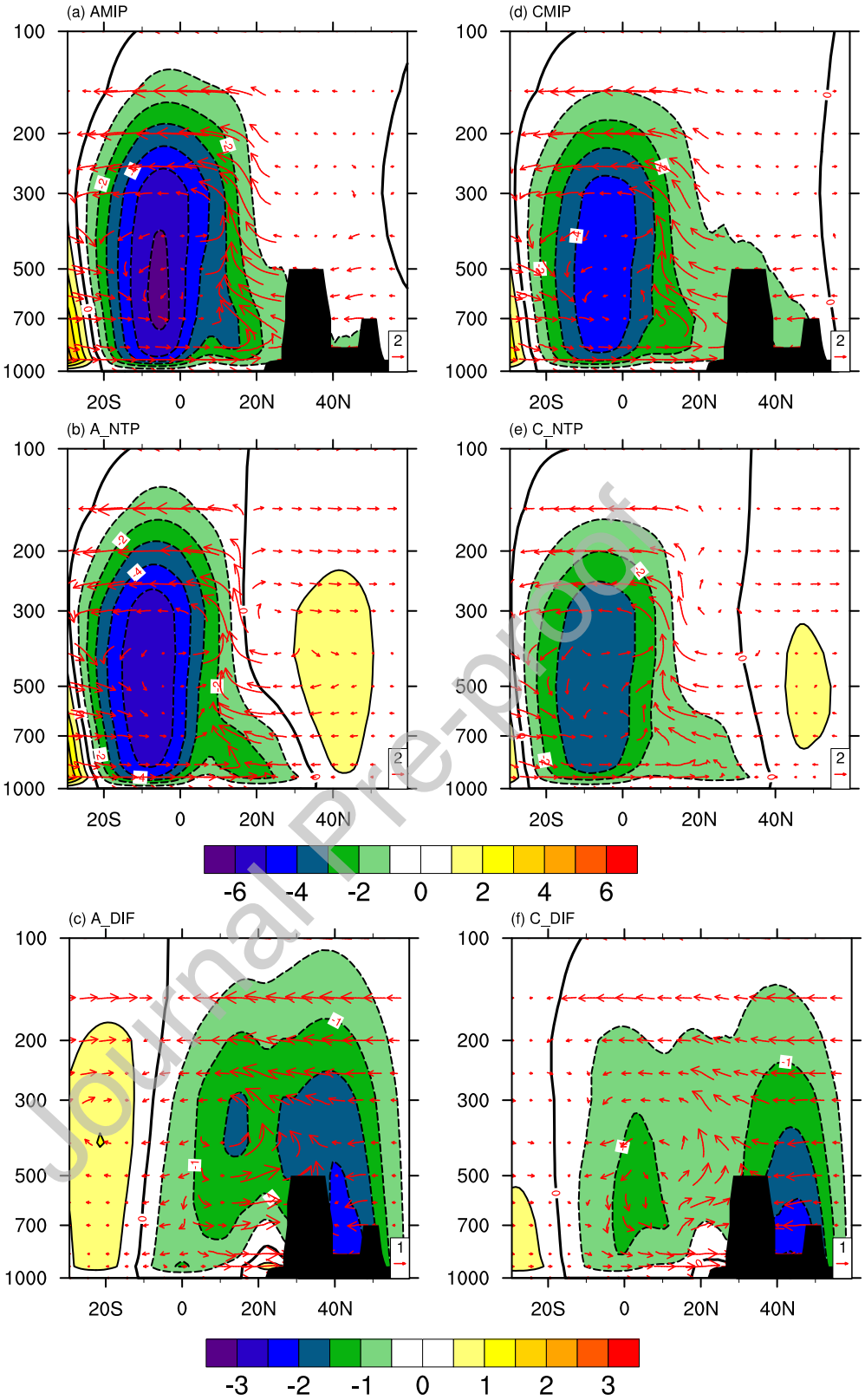

Fig. 8. Climate mean of the JJA 60-120°E zonal mean meridional stream function (shaded, 10^{11} kg s^{-1}) and winds (vectors, the vertical velocity has been scaled by 10^2, m s^{-1}) in different experiments: (a) AMIP, (b) A_NTP, (c) A_DIF, (d) CMIP, (e) C_NTP, and (f) C_DIF. The black shading denotes the topography.

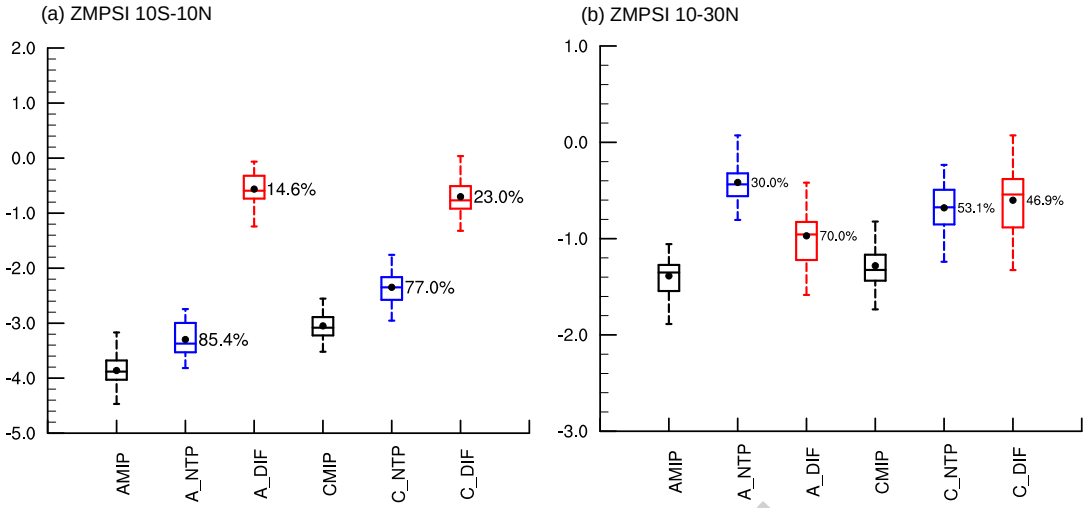

Fig. 9. Boxplot of the (a) regional mean ZMPSI (10°S-10°N, 60-120°E) and (b) regional mean ZMPSI (10-30°N, 60-120°E). The black dots denote the mean values of the datasets, and the percentages denote the mean value of the A_NTP divided by AMIP runs, and the mean value of the C_NTP divided by CMIP runs.

Table 2. Percentages of various variable changes relative to the changes in TP-SPV for the AMIP-type run and CMIP-type run as calculated in formula (3).

R(%)	R_A	R_C
TP-SPV	123%	75.50%
pr_STP	75.50%	73.60%
pr_IND	31.20%	28.40%
pr_TIO	-42.80%	-31.60%
pr_EA	20.40%	37.50%
pr_WNP	2.70%	23.10%
WYI	22.20%	43.20%
EASM_WF99	-1.40%	47.50%
EASM_WYF2001	17.60%	28.10%
ZMPSI 10S-10 N	14.6%	23.0%
ZMPSI 10-30 N	70.0%	46.9%

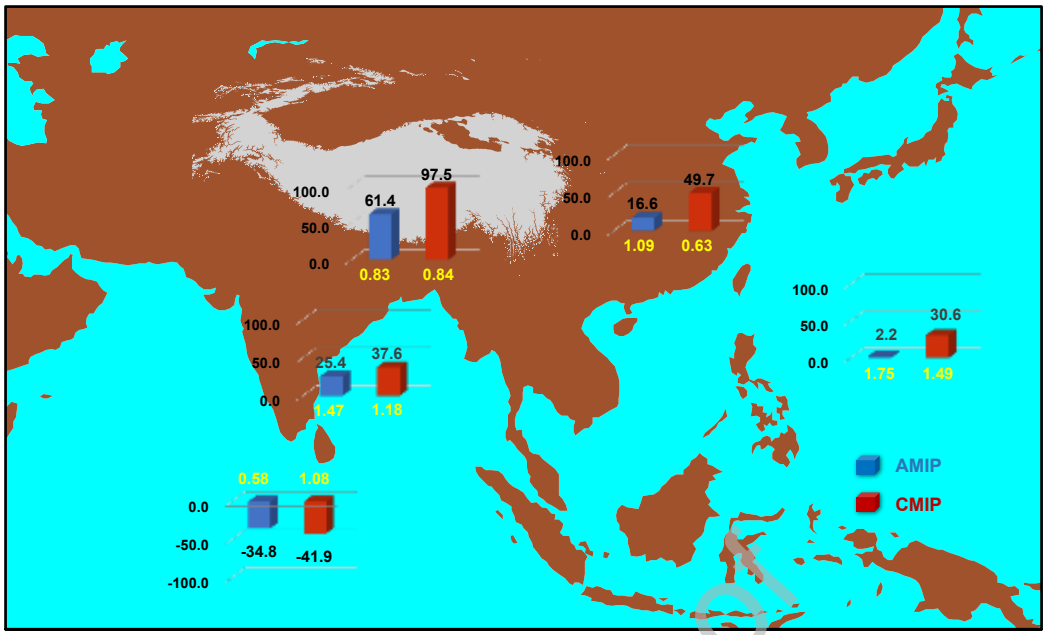

Fig. 10. Map of the relative ratio [R_{RA} and R_{RC} in formulas (5) and (6)] of monsoon precipitation responses relative to the TP-SPV changes in Table 2 for both the AMIP (blue color) and CMIP (red color) types of experiments. The black numbers above the boxes denote the ratios (%), and the yellow numbers denote the standard deviations for the precipitation changes of A_DIF and C_DIF.

Bian He received his Ph.D. degree from Nanjing University of Information Science & Technology in 2004. He is now a full professor in the State Key Laboratory of Numerical Modeling for Atmospheric Sciences and Geophysical Fluid Dynamics (LASG), Institute of

Atmospheric Physics, CAS. His research interests focus on climate dynamics and climate modeling, especially, the Tibetan Plateau and monsoon dynamics and numerical model development and application.

Graphical abstract

The thermodynamic forcing of the Tibetan Plateau (TP) is important for the regulation of the Asian summer monsoon (ASM). However, the monsoon responses to orographic perturbation simulations show controversial results in previous published literatures. In this paper, the surface potential vorticity (SPV) is used to quantify the TP surface thermodynamic forcing changes in the FGOALS-f2 climate model. The results indicate that TP-SPV is substantially reduced in the AMIP runs, while it is reduced by two-thirds of the original intensity in the CMIP runs when large-scale Asian mountains are removed. Overall, the responses of the monsoon system are more sensitive when air-sea interactions are considered. When the mountains are removed, the precipitation over the southern slope of the TP decreases by 73% and increases by nearly 30% over the tropical Indian Ocean in the CMIP runs. Moreover, the precipitation response is overall stronger in the CMIP type runs and is the largest over the south slope of the TP, and the model responses in the WNP, Indian mainland and northern Indian Ocean exhibit the highest uncertainties.

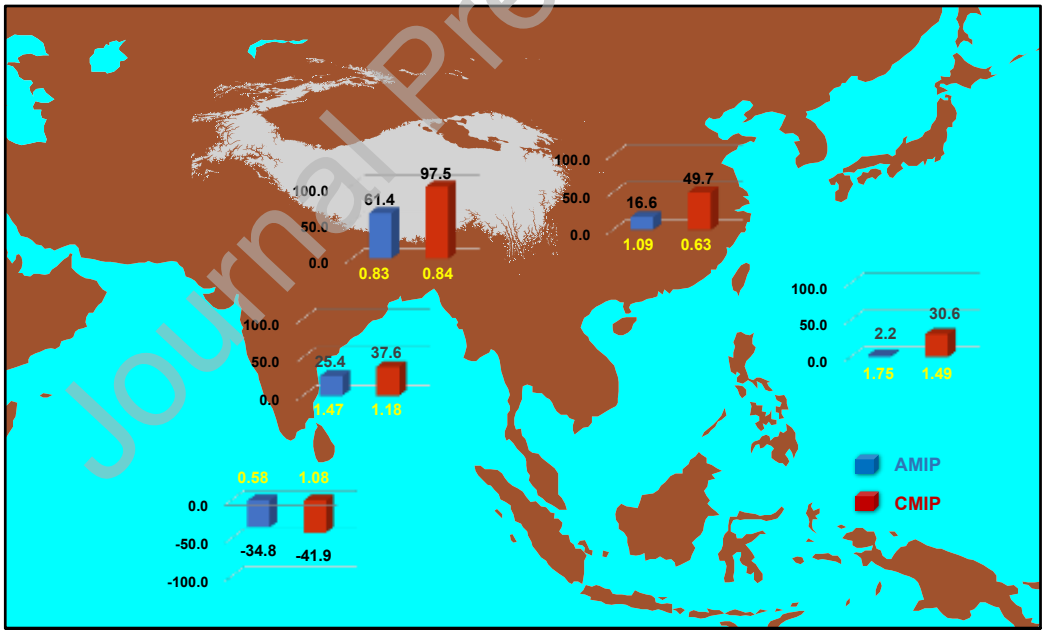

Figure Map of the ratio of monsoon precipitation responses relative to the TP-SPV changes for both the AMIP (blue color) and CMIP (red color) types of simulations. The black numbers above the boxes denote the ratios (%), and the yellow numbers denote the standard deviations.

Declaration of interests

☒ The authors declare that they have no known competing financial interests or personal relationships that could have appeared to influence the work reported in this paper.

☐The authors declare the following financial interests/personal relationships which may be considered as potential competing interests: